Inorganic Chemistry

Article

pubs.acs.org/IC

Photoluminescent 3D Lanthanide–Organic Frameworks Based on 2,5-Dioxo-1,4-piperazinylbis(methylphosphonic) Acid Formed via in Situ Cyclodehydration of Glyphosates

Yunshan Zhou,* Yan Guo, Sheng Xu, Lijuan Zhang,* Waqar Ahmad, and Zonghai Shi

State Key Laboratory of Chemical Resource Engineering, Institute of Science, Beijing University of Chemical Technology, Beijing 100029, People's Republic of China

Supporting Information

ABSTRACT: Hydrothermal reactions of lanthanide nitrates with glyphosate have resulted three new isostructural 3D lanthanide–organic frameworks, $Ln(NO_3)(H_2L)$ [Ln = Eu (**1**), Tb (**2**), Gd (**3**); H_4L = 2,5-dioxo-1,4-piperazinylbis-(methylphosphonic) acid], with good yields, where H_4L as a new ligand was formed via in situ cyclodehydration of original ligand glyphosates during the hydrothermal reaction. The compounds were thoroughly characterized by IR, UV–vis, elemental analysis, single-crystal X-ray diffraction analysis, powder X-ray diffraction analysis, and thermogravimetric/differential thermal analysis (TG-DTA). Three compounds display 3D 6,6-connected open frameworks with $4^{13}\cdot6^2$ topology possessing 1D channels in which NO_3^- anions act as troglodytes by chelating Ln^{3+} centers. The TG-DTA study of the compounds showed remarkable thermal stability up to 380 °C. Under room temperature UV-light irradiation, the Eu^{3+} and Tb^{3+} compounds showed the corresponding characteristic Ln^{3+} intra $4f^n$ emission peaks. The triplet energy level (21882 cm^{-1}) of the ligand (H_4L) was determined from the emission spectrum of its Gd^{3+} compound at 77 K. The emission lifetimes (1.54 ms of $^5D_0$ for compound **1** and 1.98 ms of $^5D_4$ for compound **2**) and absolute emission quantum yields (10.1% for compound **1** and 5.9% for compound **2**) were also determined.

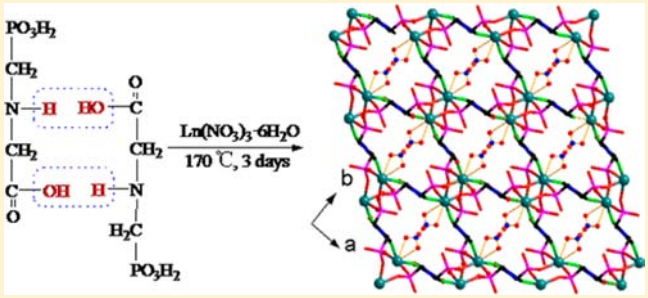

INTRODUCTION

Metal–organic phosphonate frameworks (MOPFs), formed by thermodynamically and chemically stable M–O–P bonds during the reaction of various organic phosphonates with various metals,[1] have attracted extensive interest in the last 2 decades because of their potential applications in the fields of catalytic chemistry, ion exchange, proton conductance, photoluminescence, and material chemistry.[2]

For the construction of MOPFs, the proper selection of an organic phosphate ligand with multifunctional groups is vital.[3] Existing research results show that employment of organic phosphates with –NH–, –NH═, and –COOH groups possesses a high potential to construct MOPFs with new structures and interesting properties.[4] Among organic phosphates, 2,5-dioxo-1,4-piperazinylbis(methylphosphonic) acid (H_4L), featuring a rigid six-membered ring with two carbonyl oxygen atoms of the piperazinyl ring and two phosphate groups,[5] can be the ideal organic phosphate ligand because it may show varying degrees of deprotonation just through changes in the pH of the reaction medium and therefore possesses great potential to coordinate the metal center by adopting various coordination modes through its phosphonate groups and carbonyl oxygen atoms. However, until now, there are no reports on the in situ formation of the H_4L ligand, synthesis, characterization, and applications of its complexes with either transition or lanthanide metals.

On the other hand, the hydrothermal technique is currently a common and available method to synthesize MOPFs with novel structures and promising properties.[6] To date, a large number of MOPFs with 1D, 2D, and 3D structures have been reported by using the hydrothermal technique, although controlled hydrothermal synthesis is still a challenge.[7] It is worth pointing out that direct coordination between the metal centers and organic ligands does not always simply take place; instead, sometimes the hydrothermal processes are accompanied by in situ ligand formation via hydrolysis, oxidation, hydroxylation, etc.,[6] resulting in the formation of such materials that cannot be obtained by direct synthetic assembly.[8] In situ ligand formation is not only a simple but also an environmentally friendly approach.[8] One more important thing for in situ ligand formation is that it helps us in discovering new organic reactions and understanding their mechanisms.[8] Until now, more than 10 types of in situ ligand formation reactions have been found by hydrolysis of –CN and –COOR groups,[9] hydroxylation,[10] C–C bond formation[11] etc. Therefore, in situ ligand formation has become important for organic synthesis, material science, and crystal engineering in both theoretical and practical viewpoints.[12]

Received: December 21, 2012
Published: May 20, 2013

   dx.doi.org/10.1021/ic302821w | Inorg. Chem. 2013, 52, 6338–6345

Table 1. Crystal Data and Structure Refinement for Compounds 1−3

	1	2	3
formula	$C_6H_{10}EuN_3O_{11}P_2$	$C_6H_{10}TbN_3O_{11}P_2$	$C_6H_{10}GdN_3O_{11}P_2$
fw	514.07	521.03	519.36
cryst syst	monoclinic	monoclinic	monoclinic
Space group	*C2/c*	*C2/c*	*C2/c*
a (Å)	13.710(4)	13.634(3)	13.698(3)
b (Å)	10.753(3)	10.733(2)	10.820(2)
c (Å)	9.960(3)	9.916(2)	9.954(2)
β (deg)	107.421(4)	107.274(3)	107.16(3)
V (Å^3)	1401.0(7)	1385.7(6)	1409.6(5)
Z	4	4	4
D_{calcd} (Mg/m^3)	2.437	2.498	2.447
temp (K)	103(2)	103(2)	293(2)
F(000)	992	1000	996
μ (mm^{-1})	4.771	5.401	4.998
reflns collected/unique	6338/1597	5212/1579	2589/1243
R(int)	0.0278	0.0367	0.0138
R1, wR2 [$I > 2\sigma(I)$]	0.0177, 0.0432	0.0217, 0.0514	0.0165, 0.0425
R1, wR2 (all data)	0.0192, 0.0439	0.0250, 0.0524	0.0171, 0.0427
GOF on $\|F\|^2$	0.997	1.002	1.210
largest diff peak and hole (e/Å^3)	0.618 and −0.563	1.084 and −1.232	0.664 and −0.440

In this paper, we report the preparation, characterization, and photoluminescent properties of 3D lanthanide−organic frameworks with the molecular formula $Ln(NO_3)(H_2L)$ [Ln = Eu (**1**), Tb (**2**), Gd (**3**)] based on H_4L formed via in situ cyclodehydration of glyphosates in the presence of lanthanide nitrates under hydrothermal conditions. To our best knowledge, it is the first reported in situ synthesis of H_4L, and compounds **1** and **2** represent the first photoluminescent frameworks of structurally characterized lanthanide phosphonate based on this organic phosphate ligand.

EXPERIMENTAL SECTION

Materials and Methods. $Ln(NO_3)_3{\cdot}6H_2O$ (Ln = Eu, Tb, Gd) was prepared by dissolving corresponding commercially available lanthanide oxides (99.99% purity) in nitric acid, followed by recrystallization and drying. All other materials were of reagent grade, were obtained from commercial sources, and were used without further purification. The free ligand H_4L was prepared according to the literature[5] and characterized by elemental analysis. Anal. Calcd for $C_6H_{12}N_2O_8P_2$ (H_4L): C, 23.85; H, 4.00; N, 9.27. Found: C, 23.94; H, 3.89; N, 9.18. Typical IR bands/cm^{-1} (in KBr): 3022 (m), 2837 (s), 2730 (m), 2405 (m), 1880 (w), 1741 (s), 1560 (ms), 1481 (ms), 1425 (ms), 1342 (w), 1239 (s), 1156 (s), 1091 (s), 1030 (m), 905 (s), 789 (ms), 645 (w), 575 (w), 501 (ms), 464 (ms). ^{1}H NMR (in D_2O): δ 3.64 (d, 2H, $H_2PO_3CH_2N$), 4.21 (s, 2H, $-NCH_2C{=}O$) (Figure S1 in the Supporting Information). Elemental analyses for C, H, and N were performed on a Perkin-Elmer 240C analytical instrument, while analyses for Eu, Tb, and Gd were performed using an ICPS-7500 model inductively coupled plasma emission spectrometer with all samples dissolved in dilute hydrochloric acid. IR spectra were recorded on a Nicolet FT IR-170SX spectrometer as KBr pellets in the range of 4000−400 cm^{-1}. UV−vis spectra were measured on a Shimadzu UV-2550 spectrophotometer. Thermogravimetric (TG) analyses were carried out on a NETZSCH STA 449C unit at a heating rate of 5 °C/min under air. Powder X-ray diffraction (XRD) measurements were performed on a Rigaku D/max 2500 X-ray diffractometer at a scanning rate of 15°/min in the 2θ range from 3° to 90° with graphite-monochromatized Cu Kα radiation (λ = 0.15405 nm). The excitation and emission spectra were measured with a Hitachi F-7000 FL fluorescence spectrophotometer with both excitation and emission slits of 5 nm for compounds **1** and **2** in the solid state using a 150 W xenon arc lamp as the light source. The scan rate was 1200 nm/min, and the photomultiplier tube voltage was 450 V. The photoluminescence quantum yield was measured by absolute PL quantum yield measurement system C9920-02. The luminescence decay curves were obtained from a Lecroy Wave Runner 6100 digital oscilloscope (1 GHz) using a tunable laser (pulse width 4 ns; gate 50 ns) as the excitation source (Continuum Sunlite OPO).

Synthesis of $Eu(NO_3)(H_2L)$ (1). A total of 0.233 g of $Eu(NO_3)_3{\cdot}6H_2O$ (0.5 mmol) and 0.592 g of glyphosate (3.5 mmol) were added to 15 mL of water. The resulting mixture was stirred for 3 min, then transferred to a Teflon-lined autoclave (25 mL), and kept at 170 °C for 72 h. After slow cooling to room temperature, colorless needlelike single crystals were collected, washed with distilled water, and dried at room temperature with a yield of 0.213 g (85.1% based on Eu). The initial and final pH values for the solution were measured to be 0.92 and 1.21, respectively. Anal. Calcd for $C_6H_{10}EuN_3O_{11}P_2$: C, 14.01; H, 1.95; N, 8.17; Eu, 29.38. Found: C, 14.05; H, 1.89; N, 8.10; Eu, 29.45. Typical IR bands/cm^{-1} (in KBr): 3271 (m), 2948 (w), 1661 (s), 1513 (ms), 1457 (ms), 1354 (ms), 1241 (ms), 1173 (s), 1082 (s), 919 (ms), 810 (w), 606 (ms), 447 (ms).

Synthesis of $Tb(NO_3)(H_2L)$ (2). The procedure is the same as that of compound **1** except that $Eu(NO_3)_3{\cdot}6H_2O$ is replaced by 0.226 g of $Tb(NO_3)_3{\cdot}6H_2O$ (0.5 mmol) with a yield of 0.220 g (84.51% based on Tb). The initial and final pH values for the solution were 0.97 and 1.76, respectively. Anal. Calcd for $C_6H_{10}N_3O_{11}P_2Tb$: C, 13.82; H, 1.92; N, 8.06; Tb, 30.52. Found: C, 13.78; H, 1.93; N, 8.10; Tb, 30.50. Typical IR bands/cm^{-1} (in KBr): 3263 (m), 2948 (w), 1661 (s), 1514 (ms), 1462 (ms), 1349 (ms), 1241 (ms), 1179 (s), 1094 (s), 912 (ms), 810 (w), 606 (ms), 453 (ms).

Synthesis of $Gd(NO_3)(H_2L)$ (3). The procedure is the same as that of compound **1** except that $Eu(NO_3)_3{\cdot}6H_2O$ is replaced by 0.226 g of $Gd(NO_3)_3{\cdot}6H_2O$ (0.5 mmol) with a yield of 0.215 g (82.7% based on Gd). The initial and final pH values for the solution were 0.92 and 1.70, respectively. Anal. Calcd for $C_6H_{10}N_3O_{11}P_2Gd$: C, 13.88; H, 1.94; N, 8.09; Gd, 30.28. Found: C, 13.72; H, 2.01; N, 8.01; Gd, 30.50. Typical IR bands/cm^{-1} (in KBr): 3277 (m), 2948 (w), 1661 (s), 1514 (ms), 1462 (ms), 1354 (ms), 1241 (ms), 1173 (s), 1077 (s), 918 (ms), 810 (w), 606 (ms), 453 (ms).

X-ray Crystallography. Diffraction intensities for compounds **1** and **2** were collected at 103(2) K on a computer-controlled Rigaku RAXIS-RAPID X diffractometer, and that for compound **3** was collected at 293(2) K on a computer-controlled Xcalibur E X-ray diffractometer equipped with a Saturn 70 CCD using confocal graphite-monochromated Mo Kα radiation (λ = 0.71073 Å) in the ω scan mode. The structures were solved by direct methods and refined

dx.doi.org/10.1021/ic302821w | Inorg. Chem. 2013, 52, 6338−6345

with the full-matrix least-squares technique using the *SHELXS-97* and *SHELXL-97* programs.[13] Anisotropic thermal parameters were assigned to all non-hydrogen atoms. The hydrogen atom on O3 in compound **1** and all of the hydrogen atoms in compound **3** were found in difference Fourier maps, while all of the other hydrogen atoms in compounds **1** and **2** were set in calculated positions and refined as riding atoms with a common fixed isotropic thermal parameter. The crystal data and refinement of the compounds are summarized in Table 1. Selected bond lengths and angles are listed in Table 2. Further details of the crystal structure determination have been deposited to the Cambridge Crystallographic Data Centre as supplementary publications. CCDC 904926 for compound **1**, CCDC 904925 for compound **2**, and CCDC 904927 for compound **3** contain the supplementary crystallographic data for this paper.

Table 2. Selected Bond Lengths [Å] and Angles [deg] for Compounds 1−3[a]

Compound **1**			
Eu1−O1	2.3364(18)	Eu1−O2#1	2.2997(19)
Eu1−O5	2.642(2)	Eu1−O4#4	2.3548(19)
P1−O1	1.4960(19)	P1−O2	1.4986(19)
P1−O3	1.581(2)	P1−C1	1.812(3)
O5−N2	1.268(3)	O6−N2	1.231(5)
O2#1−Eu1−O2#2	168.88(10)	O2#1−Eu1−O1	85.64(7)
O2#2−Eu1−O1	85.66(7)	O2#1−Eu1−O1#3	85.66(7)
O4#4−Eu1−O4#5	133.22(10)	O2#1−Eu1−O5#3	71.42(7)
O2#2−Eu1−O5#3	119.69(6)	O1−Eu1−O5#3	134.21(7)
O1#3−Eu1−O5#3	137.01(6)	O5#3−Eu1−O5	48.39(9)
Compound **2**			
Tb1−O2#1	2.266(2)	Tb1−O1	2.313(2)
Tb1−O4#4	2.324(2)	Tb1−O5	2.630(3)
P1−O1	1.493(2)	P1−O2	1.503(3)
P1−O3	1.582(3)	P1−C1	1.810(4)
O2#1−Tb1−O2#2	168.96(12)	O2#1−Tb1−O1#3	85.87(8)
O2#2−Tb1−O1#3	85.49(8)	O2#1−Tb1−O1	85.49(8)
O2#2−Tb1−O5#3	71.32(8)	O1#3−Tb1−O5#3	136.55(8)
O1−Tb1−O5#3	134.63(9)	O4#4−Tb1−O5#3	66.80(9)
O4#5−Tb1−O5#3	70.55(9)	O5−Tb1−O5#3	48.48(11)
Compound **3**			
Gd1−O2	2.295(2)	Gd1−O4	2.330(2)
Gd1−O5	2.349(2)	Gd1−O1	2.654(3)
O2−P1#2	1.496(2)	O6−P1	1.572(3)
O4−P1	1.492(2)	P1−C3	1.813(4)
O2#1−Gd1−O2	169.30(13)	O5−Gd1−O5#1	133.06(13)
O2#1-Gd1−O4	85.81(8)	O2#1-Gd1−O1	119.26(9)
O2−Gd1−O5#1	90.77(9)	O5−Gd1−O1#1	66.59(9)
O4−Gd1−O5#1	151.90(9)	O5#1-Gd1−O1#1	70.70(9)
O4#1-Gd1−O5#1	75.03(8)	O1−Gd1−O1#1	47.93(12)

[a]Symmetry transformations used to generate equivalent atoms. For compound **1**: #1, $x, -y+1, z+{}^1/_2$; #2, $-x+1, -y+1, -z$; #3, $-x+1, y, -z+{}^1/_2$; #4, $-x+{}^3/_2, y-{}^1/_2, -z+{}^1/_2$; #5, $x-{}^1/_2, y-{}^1/_2, z$. For compound **2**: #1, $-x+1, -y+1, -z$; #2, $x, -y+1, z+{}^1/_2$; #3, $-x+1, y, -z+{}^1/_2$; #4, $-x+{}^3/_2, y-{}^1/_2, -z+{}^1/_2$. For compound **3**: #1, $-x+1, y, -z+{}^1/_2$; #2, $-x+1, -y+2, -z$.

RESULTS AND DISCUSSION

Discussion on the Synthesis. The reactions between lanthanide nitrates and glyphosate under hydrothermal conditions resulted three new isostructural 3D lanthanide−organic frameworks, **1**−**3**, under the defined optimal conditions (Ln^{3+}:H_2L = 1:7, pH = 0.9, temperature = 170 °C, and time = 72 h) with high yield (>80%). The original glyphosate ligand underwent cyclodehydration during the hydrothermal reaction to form the new ligand H_4L, which concomitantly coordinated with Ln^{3+} centers to form the resulting lanthanide−organic frameworks **1**−**3**. The proposed mechanism for the formation of the ligand is shown in Scheme 1a. The cyclodehydration conditions of glyphosate were investigated systematically in the presence and absence of Ln^{3+} with different molar ratios of glyphosate to Ln^{3+} under different temperatures. The results show that only partial glyphosate was transformed into the ligand H_4L in either the presence or absence of Ln^{3+} conditions. The in situ formed ligand H_4L simultaneously coordinated to Ln^{3+}, forming compounds **1**−**3** in the presence of Ln^{3+}, while the unchanged glyphosate was left in the reaction solution. Large amounts of pure crystals of compounds **1**−**3** were harvested under the optimum conditions (molar ratio 3.5:1 of glyphosate/Ln^{3+}; temperature range of 160−170 °C). The remainder in the mother liquid was a mixture of glyphosate and the ligand H_4L. The results indicate that Ln^{3+} did not catalyze cyclodehydration of glyphosate and that Ln^{3+} preferred to coordinate the ligand H_4L rather than glyphosate when both glyphosate and the ligand H_4L were present. Interestingly, our previous work[14] showed that when a second ligand (oxalate) was added into the lanthanide nitrates and glyphosate mixture, no cyclodehydration was observed; instead, both oxalate and glyphosate ligands were found to bind with Ln^{3+} cations, forming two isomorphous 3D lanthanide oxalatophosphonate frameworks, **4** and **5** (Scheme 1b). However, it is unclear at the moment about the mechanism involved in cyclodehydration of glyphosate.

This indicates that the presence of oxalate prevented the glyphosate from cyclodehydration. Therefore, it is concluded

Scheme 1. Schematic View of in Situ Generation of H_4L under Hydrothermal Conditions and the Simultaneous Formation of Compounds 1−3 (a) and the Formation of Compounds 4 and 5 in the Presence of Oxalic Acid (b)

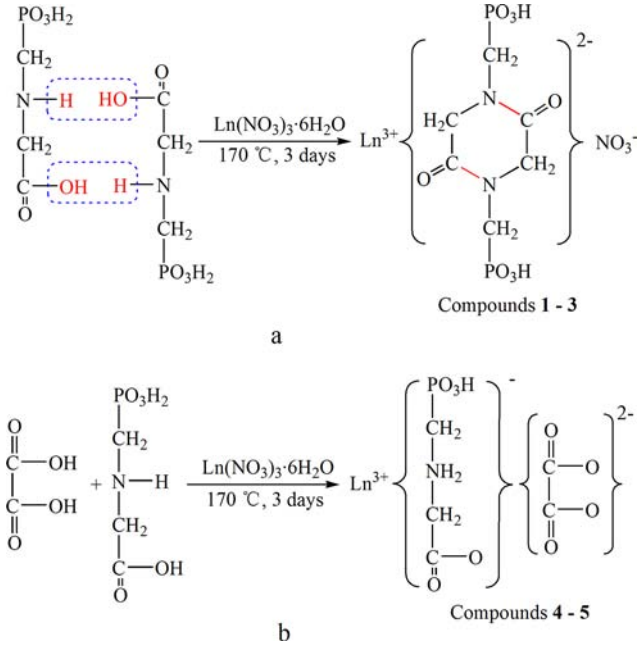

dx.doi.org/10.1021/ic302821w | *Inorg. Chem.* 2013, 52, 6338−6345

that the types of starting materials and their molar ratio play key roles in determing the composition and structure of the final products.

Crystal Structures of Compounds 1−3. The powder XRD patterns of compounds **1**−**3** are essentially in agreement with those simulated from single-crystal XRD data (Figures S2−S4 in the Supporting Information), which indicate the homogeneous phases of the final products. No other peaks can be found in the pattern, revealing that there is no impurity in the products. On the basis of the powder XRD patterns, compounds **1**−**3** are confirmed to be isomorphous, which is consistent with the single-crystal XRD analysis described below.

Because single-crystal XRD analysis reveals that compounds **1**−**3** are isomorphous, only the structure of compound **1** will be discussed in detail as a representation. As shown in Figure 1, Eu^{III} is eight-coordinated, with a distorted dodecahedron geometry environment, by eight oxygen atoms, including four phosphonate oxygen atoms (O1, O1#2, O2#3, and O2#5) of four different H_2L^{2-} ligands, two oxygen atoms (O4#1 and O4#4) from carbonyl groups of two different H_2L^{2-} ligands, and two oxygen atoms from one nitrate. The Eu−O bond lengths are in the range of 2.2997(19)−2.642(2) Å, and the O−Eu−O bond angles vary from 48.39(9) to 168.88(10)° (Table 2). All bond lengths and angles are within the normal range and are in agreement with the literature.[15] It is noteworthy that there is no water molecule either in the coordination environment of Eu^{III} or in the lattice structure of compound **1**.

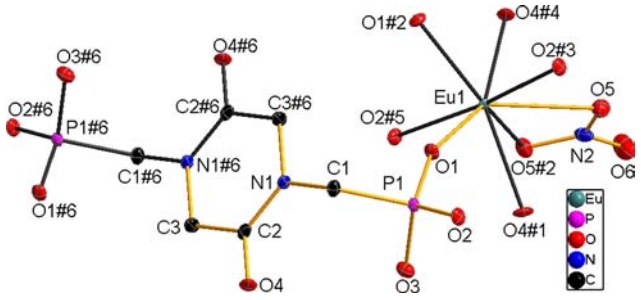

Figure 1. Perspective view of the local coordination environment of the Eu^{III} ion in compound **1** with thermal ellipsoids drawn at the 50% probability level showing the labeling scheme (hydrogen atoms are omitted for clarity). Symmetry transformations used to generate equivalent atoms: #1, $x, -y + 1, z + {}^1/_2$; #2, $-x + 1, -y + 1, -z$; #3, $-x + 1, y, -z + {}^1/_2$; #4, $-x + {}^3/_2, y - {}^1/_2, -z + {}^1/_2$; #5, $x - {}^1/_2, y - {}^1/_2, z$; #6, $x + {}^1/_2, y + {}^1/_2, z$; #7, $-x + {}^3/_2, -y + {}^3/_2, -z + 1$.

In compound **1**, all of the H_2L^{2-} ligands adopt a 6-connected coordination mode (Figure S5 in the Supporting Information). The O1 and O2 atoms from each phosphonate group are coordinated to two Eu^{3+} ions with a Eu1−O1 bond length of 2.3364(18) Å and a Eu1−O2 bond length of 2.2997(19) Å, and each carbonyl O4 from the piperazine ring is coordinated to one Eu^{3+} ion with a Eu−O4 bond length of 2.3548(19) Å (Table 2).

The 3D open framework of compound **1** can be described as follows: the H_2L^{2-} ligands and Eu^{III} pairs (the Eu···Eu distance within the Eu^{III} pair is 5.78 Å) connect to each other alternately, forming a 1D infinite chain in the *ac* plane by forming coordination bonds between oxygen atoms (O1 and O2) from phosphate groups and Eu^{3+} ions (Figure 2a). The shortest distance of the adjacent Eu^{III} pairs is ca. 10.95 Å. The adjacent 1D chains then joined together by forming coordination bonds between carbonyl oxygen atoms (O4) of the piperazine ring of H_2L^{2-} ligands and Eu^{3+} ions, forming a 2D Eu−H_2L^{2-} layer in the *ac* plane, with the shortest Eu···Eu separation being ca. 5.78 Å between the adjacent 1D Eu−H_2L^{2-} chains (Figure 2b). The 2D Eu−H_2L^{2-} layers are further linked by 6-connected H_2L^{2-} ligands through coordination bonds

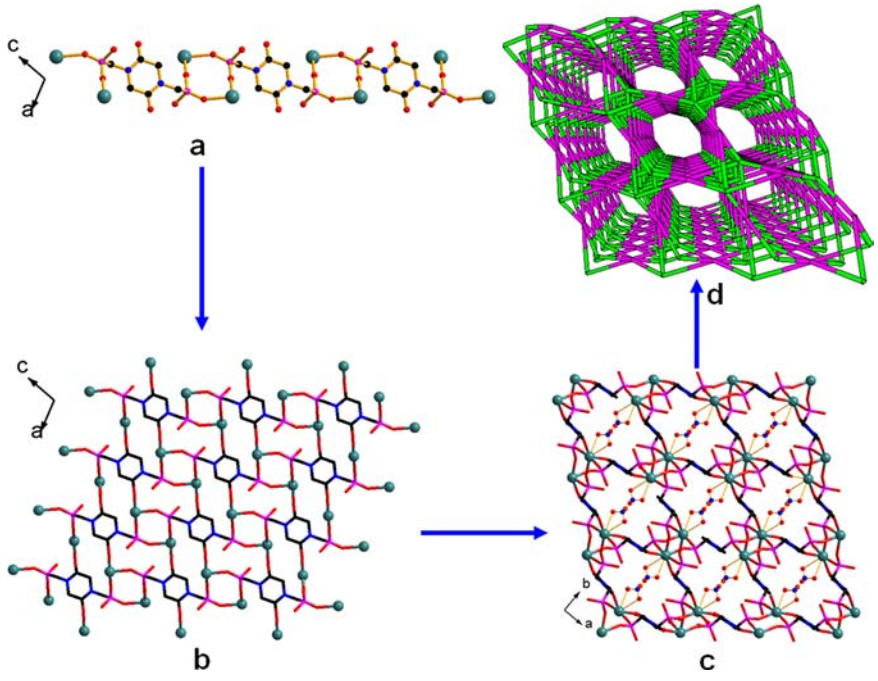

Figure 2. 1D chain composed of H_2L^{2-} and Eu^{3+} in the *ac* plane (a), 2D plane composed of 1D chains in the *ac* plane (b), 3D open-framework structure possessing 1D channels in which nitrates reside via chelating Eu^{3+} ions (c), and 3D topological representation with $4^{13}{\cdot}6^2$ topology (d) in compound **1**. All hydrogen atoms were omitted for clarity.

dx.doi.org/10.1021/ic302821w | *Inorg. Chem.* 2013, 52, 6338−6345

between Eu^{3+} ions and the oxygen atoms (O1, O2, and O4), resulting in a complex 3D open framework with 1D channels along the *c* axis (Figure 2c), in which the shortest interlayer Eu···Eu contact is ca. 7.57 Å. The nitrates, all having bidentate chelating coordination mode, reside in the 1D channels via chelating Eu^{3+} ions (Figure 2c).

For a better understanding of the 3D structure of compound **1**, topological analysis was carried out. The Eu^{3+} ion is viewed as a node, which links six H_2L^{2-} ligands; therefore, it is regarded as a hexa-corner-share holder, and each H_2L^{2-} ligand links six Eu^{3+} ions (Figure S5 in the Supporting Information) and therefore is also considered as a hexa-corner-share holder. Such connectivity repeats infinitely to give the 3D framework of **1**, as schematically shown in Figure 2d. According to the simplification principle,[16] the resulting structure of **1** is a binodal 6,6-connected net with its point (Schläfli) symbol of $4^{13}\cdot6^2$. Although compound **1** exhibits an interesting complicated 3D framework structure (Figure 2d), 0% solvent-accessible volume has been calculated from the *CALC SOLV* command in *PLATON*.[17] The complex packing arrangements of nitrates are blocking the void space of the framework channels.

IR Spectra of Compounds 1−3. The IR spectra of compounds **1**−**3** are shown in Figure S6 in the Supporting Information. The IR spectra of the three compounds are nearly the same because of their isomorphous nature; thus, only the spectrum of compound **1** will be interpreted. The broad band in the range of 3450−3000 cm^{-1} centered at 3271 cm^{-1} corresponds to the OH stretching vibrations of phosphonate groups. The strong band centered at 1661 cm^{-1} is assigned to the stretching vibrations of C═O from amide groups of the H_2L^{2-} ligand.[18] The band at 1354 cm^{-1} is due to the stretching vibrations of C−N of the ligand.[19] Furthermnore, three strong bands at 1241, 1082, and 919 cm^{-1} are due to the stretching vibrations of the tetrahedral CPO_3 groups, as expected.[20]

UV−Vis Absorption Spectrum of H_4L. The UV−vis absorption spectrum of H_4L shows two absorption bands at 211and 256 nm (Figure S7 in the Supporting Information), which are assigned to an n → π^* amide transition of the piperazine ring. Molar extinction coefficient values at 211 and 256 nm are 1.0×10^4 and 6.8×10^3 L/mol·cm, respectively, indicating that the ligand is an adequate light-harvesting chromophore for the sensitization of lanthanide luminescence.[21]

Diffuse-Reflectance Spectroscopy. The diffuse-reflectance spectra of compounds **1**−**3** and of free ligand H_4L are shown in Figure S8 in the Supporting Information. The ligand displays two absorption bands in the UV region at 224 and 289 nm, which are assigned to singlet−singlet n → π^* absorptions of the amide bond. The spectra of compounds **1**−**3** are similar to the one observed for the free ligand, implying that the singlet excited state of the free ligand is not significantly affected by complexation of the Ln^{3+} ion. However, a small blue shift that is discernible in the absorption maximum of the compounds is attributable to the perturbation induced by the metal coordination.[22] Therefore, the observed bands in the UV region of the prepared compounds and of the ligand can be assigned to electronic transitions from the ground-state level S_0 to the excited-state level S_1 of H_4L.

Photoluminescence Properties of Compounds 1 and 2. According to Reinhoudt's empirical rule,[23] the intersystem crossing process becomes effective when the energy gap between the singlet ($^1\pi\pi^*$) and triplet ($^3\pi\pi^*$) energy levels of a ligand $\Delta E(^1\pi\pi^*-{}^3\pi\pi^*)$ is greater than the lowest value of 5000 cm^{-1}. The singlet-state energy level of H_4L was estimated by referencing its absorbance edge, which was 34965 cm^{-1} (286 nm) based on the UV−vis absorption spectrum of H_4L (Figure S7 in the Supporting Information). Because the lowest excited state $^6P_{7/2}$ of the Gd^{III} ion is too high to accept energy from a ligand, the data obtained from the phosphorescence spectrum of the corresponding gadolinium compound based on the ligand actually reveal the triplet energy level of the corresponding ligand.[24] Thus, the triplet-state energy ($^3\pi\pi^*$) level of H_4L was found to be 21882 cm^{-1} (457 nm) based on the low-temperature (77 K) phosphorescence spectrum of compound **3** (Figure S9 in the Supporting Information).[25] Therefore, the energy gap $\Delta E(^1\pi\pi^*-{}^3\pi\pi^*)$ is calculated to be 13143 cm^{-1} for H_4L, indicating that the intersystem crossing process in both compounds **1** and **2** is effective.

In addition, according to the intramolecular energy-transfer mechanism,[26] the intramolecular energy transfer includes the following two energy-transfer processes: the energy transfer from the lowest triplet energy level of the ligand to the resonant energy level of the lanthanide ion by Dexter's resonant exchange interaction and the inverse energy transfer from the lanthanide ion to the organic ligand by a thermal deactivation mechanism.[21] Both energy-transfer processes depend on the energy gap between the lowest triplet energy level of the organic ligand and the resonant energy level of the lanthanide ion. An optimal value of the energy gap is assumed to exist around 3000 ± 500 cm^{-1}.[23] Either a larger or a smaller energy difference may result in a decrease of the luminescent intensities of lanthanide complexes. However, some factors, such as the oscillation of coordinated water molecules, can also affect the photoluminescent properties of lanthanide complexes that are not included into the estimation, so the estimated optimal value may not be accurate.[23] The energy difference (3208 cm^{-1}) between the lowest triplet state of H_4L (21882 cm^{-1}) and the resonant energy level of Eu^{3+} ($^5D_1$, 18674 cm^{-1}) exists within the optimal value, indicating that H_4L is suitable for luminescence of Eu^{3+}. Oppositely, the energy difference (1382 cm^{-1}) between the lowest triplet state of H_4L (21882 cm^{-1}) and the resonant energy level of Tb^{3+}($^5D_4$, 20500 cm^{-1}) is a little far from the optimal value of the energy gap assumed to exist around 3000 ± 500 cm^{-1}, leading to increased inverse energy transfer from the resonant emissive energy level of $^5D_4$ of Tb^{3+} to the lowest triplet state of the H_4L ligand. Therefore, it can be expected that compound **1** may display better luminescent properties than compound **2**.

The room temperature luminescent properties of compounds **1** and **2** were investigated in the solid state. Figure 3a shows the room temperature excitation spectrum of **1** monitored around the more intense emission line, 590 nm, for Eu^{3+}. The excitation spectrum shows a broad band in the region of 210−290 nm (peak centered at 257 nm) ascribed to the electronic transitions of the H_4L ligand, with the $^7F_0 \rightarrow {}^5F_4$ (297 nm), $^7F_0 \rightarrow {}^5H_6$ (319 nm), $^7F_0 \rightarrow {}^5D_4$ (361 nm), $^7F_0 \rightarrow {}^5G_2$ (381 nm), $^7F_0 \rightarrow {}^5L_6$ (392 nm), $^7F_0 \rightarrow {}^5D_3$ (414 nm), $^7F_0 \rightarrow {}^5D_2$ (464 nm), $^7F_0 \rightarrow {}^5D_0$ (525 nm), $^7F_1 \rightarrow {}^5D_0$ (534 nm) transitions[24] of the Eu^{3+} ion also being detected. Detection of the band (257 nm), together with its higher intensity relative to the intra $4f^6$ transitions, implies a more effective luminescence sensitization via the ligand excited states than that of the direct intra $4f^6$ excitation.[25] The room temperature emission spectrum (Figure 3b) of compound **1** excited at 257 nm (the maximum excitation wavelength) exhibits a series of straight lines assigned

dx.doi.org/10.1021/ic302821w | *Inorg. Chem.* 2013, 52, 6338−6345

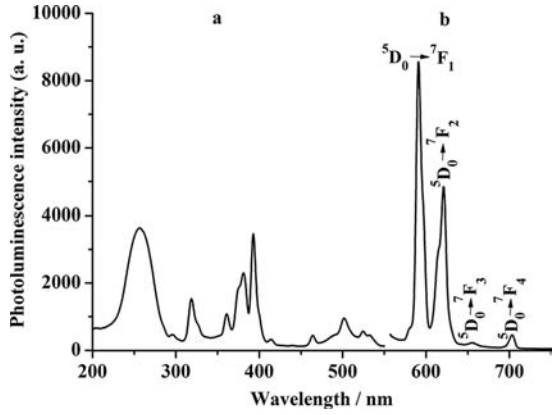

Figure 3. Solid-state excitation (λ_{em} = 590 nm; a) and emission (λ_{ex} = 257 nm; b) spectra of compound **1**.

to intra 4f^6 ($^5D_0 \rightarrow {}^7F_1$, $^5D_0 \rightarrow {}^7F_2$, $^5D_0 \rightarrow {}^7F_3$, and $^5D_0 \rightarrow {}^7F_4$) transitions of the Eu^{3+} ion with maxima at 590, 614, 656, and 704 nm.[26] Luminescence from higher excited states, such as $^5D_1$, is not detected, indicating efficient nonradiative relaxation to the $^5D_0$ level. The $^5D_0 \rightarrow {}^7F_1$ transition is a magnetic-dipole transition, and its intensity varies with the crystal-field strength imposed on the Eu^{3+} ions. The $^5D_0 \rightarrow {}^7F_2$ transition is an electric-dipole transition, and the intensity of this transition decreases as the site symmetry of the Eu^{3+} ions increases.[27] The most intense transition is $^5D_0 \rightarrow {}^7F_1$, which implies intense orange luminescence. The higher intensity of the $^5D_0 \rightarrow {}^7F_1$ transition with respect to the electric dipole $^5D_0 \rightarrow {}^7F_2$ indicates that the local symmetry group around the metal ions has a high symmetry with an inversion center,[28] which was already confirmed by single-crystal XRD analysis of the structure of the compound as described above.

The room temperature excitation spectrum of compound **2** (Figure 4a) monitored around the more intense emission line,

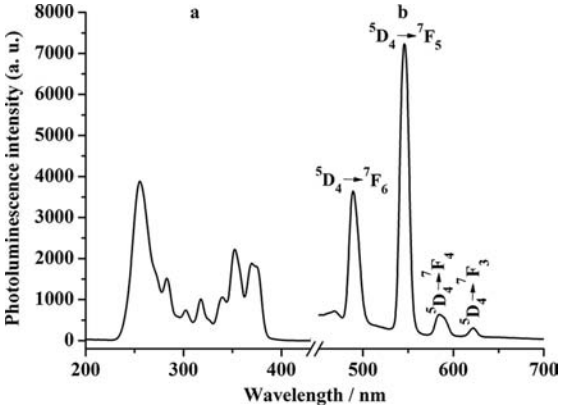

Figure 4. Solid-state excitation (λ_{em} = 545 nm; a) and emission (λ_{ex} = 256 nm; b) spectra of compound **2**.

545 nm, for Tb^{3+} shows a large broad band in the region of 230−310 nm (peak centered at 256 nm) ascribed to the electronic transitions of the H_2L^{2-} ligand, and the sharp lines between 300 and 500 nm correspond to the $^7F_6 \rightarrow {}^5D_0$, $^7F_6 \rightarrow {}^5G_{2-6}$, $^5L_{10}$, and $^5D_{2-3}$ (at 302, 317, 338, 352, 369, and 375 nm) intraconfigurational forbidden 4f$^8 \rightarrow$ 4f^8 transitions of the Tb^{3+} ion[24] also being detected. Compound **2** emits green light in the solid state, and the luminescence emission spectrum were measured upon excitation at 256 nm (the maximum excitation wavelength). As shown in Figure 4b, the characteristic transitions of the Tb^{III} ion from the emitting level ($^5D_4$) to the ground-state multiplet ($^7F_{6-3}$) are observed.[29] The $^5D_4 \rightarrow {}^7F_5$ transition is the strongest emission at 546 nm, the $^5D_4 \rightarrow {}^7F_6$ transition is the second largest emission at 488 nm, and the $^5D_4 \rightarrow {}^7F_3$ transition is the weakest peak at 623 nm.

It is worth pointing out that, in general, organic ligands cannot completely encapsulate all of the Ln^{3+} ions but leave several sites to bind with the solvent molecules under hydrothermal conditions,[30] and as a consequence, a weak vibronic coupling between lanthanides and OH oscillators of coordinated water molecules normally provides a facile path for radiationless deexcitation of the Ln^{3+} ion.[31] Chemists tried to reduce the OH variation by changing OH to OD or OF or removing the water molecules from the compounds to enhance the luminescent intensity of the Ln^{III} compounds.[32] Remarkably, the Eu^{3+} and Tb^{3+} ions in compounds **1** and **2** have their coordination spheres fully occupied by the H_2L^{2-} ligands and nitrate (Figure 1) without any water molecules, consequently leading to the strong orange luminescence in the solid in compound **1** and green luminescence in compound **2**.

The $^5D_0$ (Eu^{3+}) and $^5D_4$ (Tb^{3+}) decay curves were monitored within the more intense line of the $^5D_0 \rightarrow {}^7F_1$ and $^5D_4 \rightarrow {}^7F_5$ transitions, respectively, with excitations in the intra 4f^N levels (464 nm for **1** and 490 nm for **2**). The room temperature emission decay curves of compounds **1** (Figure S10 in the Supporting Information) and **2** (Figure S11 in the Supporting Information) are well fitted by a single-exponential function. The determined emission lifetimes of compounds **1** and **2** are 1.54 and 1.98 ms, respectively. These values are found among the highest ones for lanthanide−organic frameworks.[22,33]

According to the well-established photophysical model that explains the sensitization pathway in a luminescent lanthanide complex, the absolute emission quantum yield (Φ_{tot}) of ligand-sensitized lanthanide emission, experimentally determined, is the product of the ligand sensitization efficiency (η_{sens}) and the intrinsic quantum yield (Φ_{Ln}) of the lanthanide luminescence according to[34]

$$\Phi_{tot} = \eta_{sens}\Phi_{Ln} \quad (1)$$

The energy-transfer efficiency (η_{sens}) is the product of the two processes involving intersystem crossing from the first excited singlet state of the ligand to the triplet state and energy transfer to the lanthanide. The intrinsic quantum yield of the lanthanide luminescence step (Φ_{Ln}) can be evaluated on the basis of the experimentally observed emission lifetime (τ_{obs}) and pure radiative lifetime (τ_R) of the Eu^{III} $^5D_0 \rightarrow {}^7F_J$ (J = 0−4) transitions by using[35]

$$\Phi_{Ln} = \tau_{obs}/\tau_R \quad (2)$$

$$1/\tau_R = A_{MD,0}n^3(I_{tot}/I_{MD}) \quad (3)$$

where $A_{MD,0}$ = 14.65 s^{-1} is the spontaneous emission probability of the $^5D_0 \rightarrow {}^7F_1$ transition of Eu^{III}, n the refractive index of the medium, I_{tot}/I_{MD} the ratio of the integrated total area of the corrected Eu^{III} emission spectrum to the area of the magnetic-dipole $^5D_0 \rightarrow {}^7F_1$ transition. Table 3 presents the radiative lifetimes (τ_R), intrinsic quantum yields of the lanthanide luminescence step (Φ_{Ln}), sensitization efficiencies (η_{sens}), emission lifetimes (τ_{obs}), and absolute emission quantum yields (Φ_{tot}) of compounds **1** and **2**.

dx.doi.org/10.1021/ic302821w | Inorg. Chem. 2013, 52, 6338−6345

Table 3. Radiative Lifetimes (τ_R), Intrinsic Quantum Yields of the Lanthanide Luminescence Step (Φ_{Ln}), Sensitization Efficiencies (η_{sens}), Emission Lifetimes (τ_{obs}), and Absolute Emission Quantum Yields (Φ_{tot}) of Compounds 1 and 2

compound	τ_R(ms)	τ_{obs}(ms)	Φ_{Ln}(%)	η_{sens}(%)	Φ_{tot}(%)
1	11.36	1.54	12.33	81.91	10.1
2		1.98			5.90

Thermal Properties. In order to investigate the thermal stability of the compounds, TG-DTA analyses were conducted for compounds **1** and **2**. It was found that they showed similar one-step weight loss profiles (Figure 5). Remarkably, the compounds possess good thermal stability up to 380.0 °C due to the absence of both aqua ligands and lattice water molecules in the compounds. The stability is very important in view of materials science. After 380.0 °C, the compounds start to decompose, with weight losses of 19.51% (calcd 19.84%) for compound **1** and 18.94% (calcd 19.58%) for compound **2** between 380 and 590 °C, corresponding to the remainder with the stoichiometric formula of $C_4H_{10}EuN_2O_7P_2$ for compound **1** and $C_4H_{10}N_2O_7P_2Tb$ for compound **2**, respectively. Correspondingly, the weight loss processes are accompanied by two distinct exothermal DTA peaks at 418.2 and 510.9 °C for compound **1** and at 430.5 and 599.5 °C for compound **2**.

CONCLUSION

Three new 3D lanthanide–organic frameworks, $Ln(NO_3)(H_2L)$ (Ln = Eu, Tb, Gd), have been prepared successfully under hydrothermal conditions. The original glyphosate ligand was transformed to H_4L, which was for the first time synthesized by in situ hydrothermal conditions. This method provided not only a new approach for the synthesis of H_4L but also possibilities to synthesize other Ln^{3+}-containing compounds in order to investigate other potential interesting chemophysical properties. All of the compounds described in this work showed high thermal stability from 25 to 380 °C. Compounds **1** and **2** showed strong orange and green photoluminescence due to the absence of aquo ligands around Eu^{3+}/Tb^{3+} coordination spheres, respectively. The study of the photoluminescence of compounds **1** and **2** indicated that H_4L is more suitable for the sensitization of Eu^{3+} luminescence than Tb^{3+} luminescence and can transfer energy more efficiently to Eu^{3+}. Emission lifetimes of 1.54 ms ($^5D_0$, for **1**) and 1.98 ms ($^5D_4$, for **2**) and absolute emission quantum yields of 10.1% for compound **1** and 5.9% for compound **2** were obtained. A high efficiency of the ligands-to-Eu^{3+} energy transfer was estimated as 81.91% for compound **1**. The merit of high thermal stability, strong emission, and long emission lifetime may qualify compounds **1** and **2** as highly attractive candidates for photoluminescent materials.

ASSOCIATED CONTENT

Supporting Information

X-ray crystallographic files in CIF format, ^1H NMR and IR spectra, a UV–vis spectrum of H_4L, a phosphorescence spectrum of **3**, room temperature emission decay curves of compounds **1** and **2**, and solid-state diffuse-reflectance spectra and powder XRD patterns of compounds **1**–**3**. This material is available free of charge via the Internet at http://pubs.acs.org.

AUTHOR INFORMATION

Corresponding Author

*E-mail: zhouys@mail.buct.edu.cn or zhouyun0734@sina.com.cn (Y.Z.), ljzhang@mail.buct.edu.cn (L.Z.).

Author Contributions

The manuscript was written through contributions of all authors. All authors have given approval to the final version of the manuscript.

Notes

The authors declare no competing financial interest.

ACKNOWLEDGMENTS

Financial support from the National Natural Science Foundation of China (Grant 20975009) and PCSIRT (Grant IRT1205) is greatly acknowledged.

REFERENCES

(1) John, A. G.; Paul, A. W.; Philip, L. *Inorg. Chem.* **2005**, *44*, 1736–1739.
(2) Sharma, C. V. K.; Clearfield, A. *J. Am. Chem. Soc.* **2000**, *122*, 4394–4402.
(3) Camargo, M. A.; Neve, A.; Szpoganicz, B.; Bortoluzzi, A. J.; Fischer, F. L.; Terenzi, H.; Castellano, E. E. *Inorg. Chem.* **2010**, *49*, 3057–3063.
(4) Gemmill, W. R.; Smith, M. D.; Reisner, B. A. *J. Solid State Chem.* **2005**, *178*, 2658–2662.
(5) Shkolnikoval, M.; Kirschs, G.; Sotmans, S. *Sov. Phys. Crystallogr.* **1992**, *37*, 59–62.

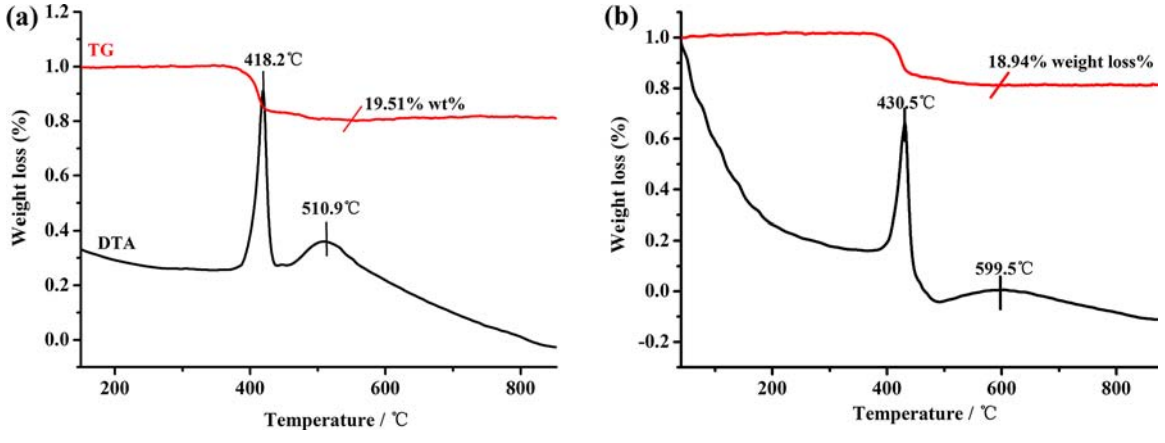

Figure 5. TG-DTA curves of compounds **1** (a) and **2** (b).

dx.doi.org/10.1021/ic302821w | *Inorg. Chem.* 2013, 52, 6338–6345

(6) Liu, F.; Duan, L.; Li, Y.; Wang, E.; Wang, X.; Hu, C.; Xu, L. *Inorg. Chim. Acta* **2004**, *357*, 1355−1359.
(7) (a) Attfield, M. P.; Yuan, Z.-H.; Harvey, H. G.; Clegg, W. *Inorg. Chem.* **2010**, *49*, 2656−2666. (b) Shi, F. N.; Cunha-Silva, L.; Sá Ferreira, R. A.; Mafra, L.; Trindade, T.; Carlos, L.; Paz, F. A. A.; Rocha, J. *J. Am. Chem. Soc.* **2008**, *130*, 150−167. (c) Zhu, Y.; Sun, Z.; Chen, H.; Zhang, J.; Zhao, Y.; Zhang, N.; Liu, L.; Lu, X.; Wang, W.; Tong, F.; Zhang, L. *Cryst. Growth Des.* **2009**, *7*, 3228−3234.
(8) (a) Sun, J.; Li, L.; Zheng, X. *Inorg. Chem. Commun.* **2011**, *14*, 877−881. (b) Han, Z. G.; Gao, Y. Z.; Zhai, X. L.; Song, H. H. *Inorg. Chem. Commun.* **2007**, *10*, 1079−1082. (c) Rowland, C. E.; Belai, N.; Knope, K. E.; Cahill, C. L. *Cryst. Growth Des.* **2010**, *10*, 1390−1398.
(9) (a) Kong, X.-J.; Zhuang, G.-L.; Ren, Y.-P.; Long, L.-S.; Huang, R.-B.; Zheng, L.-S. *Dalton Trans.* **2009**, 1707−1709. (b) Lin, W.; Evans, O. R.; Xiong, R.-G.; Wang, Z. *J. Am. Chem. Soc.* **1998**, *120*, 13272−13273. (c) Evans, O. R.; Wang, Z.; Xiong, R.-G.; Foxman, B. M.; Lin, W. *Inorg. Chem.* **1999**, *38*, 2969−2973. (d) Evans, O. R.; Lin, W. *Acc. Chem. Res.* **2002**, *35*, 511−522. (e) Ye, Q.; Li, Y.-H.; Song, Y.-M.; Huang, X.-F.; Xiong, R.-G.; Xue, Z. *Inorg. Chem.* **2005**, *44*, 3618−3625. (f) Chen, X.-M.; Tong, M.-L. *Acc. Chem. Res.* **2007**, *40*, 162−170. (g) Zhang, X.-M. *Coord. Chem. Rev.* **2005**, *249*, 1201−1219. (h) Zhang, J.-P.; Lin, Y.-Y.; Huang, X.-C.; Chen, X.-M. *J. Am. Chem. Soc.* **2005**, *127*, 5495−5506. (i) Cheng, L.; Zhang, W.-X.; Ye, B.-H.; Lin, J.-B.; Chen, X.-M. *Inorg. Chem.* **2007**, *46*, 1135−1143. (j) Zhang, J.-P.; Chen, X.-M. *Chem. Commun.* **2006**, 1689−1699. (k) Wang, Y.-T.; Fan, H.-H.; Wang, H.-Z.; Chen, X.-M. *Inorg. Chem.* **2005**, *44*, 4148−4150. (l) Huang, X.-C.; Zheng, S.-L.; Zhang, J.-P.; Chen, X.-M. *Eur. J. Inorg. Chem.* **2004**, *5*, 1024−1025.
(10) (a) Lin, W.-B.; Evans, O. R.; Xiong, R.-G.; Wang, Z.-Y. *J. Am. Chem. Soc.* **1998**, *120*, 13272−13274. (b) Lin, W.-B.; Wang, Z.-Y.; Ma, L. *J. Am. Chem. Soc.* **1999**, *121*, 11249−11250. (c) Evans, O. R.; Lin, W. *Chem. Mater.* **2001**, *13*, 3009−3017. (d) Evans, O. R.; Lin, W. *Chem. Mater.* **2001**, *13*, 2705−2712.
(11) (a) Zhang, X.-M.; Tong, M.-L.; Chen, X.-M. *Angew. Chem., Int. Ed.* **2002**, *41*, 1029−1031. (b) Zhang, X.-M.; Tong, M.-L.; Gong, M.-L.; Lee, H.-K.; Luo, L.; Li, K.-F.; Tong, Y.-X.; Chen, X.- M. *Chem.—Eur. J.* **2002**, *8*, 3187−3194.
(12) (a) Evans, O. R.; Lin, W. *Cryst. Growth Des.* **2001**, *1*, 9−11. (b) Xiong, R.-G.; Zhang, J.; Chen, Z.-F.; You, X.-Z.; Che, C.-M.; Fun, H.-K. *J. Chem. Soc., Dalton Trans.* **2001**, *6*, 780−782.
(13) (a) Sheldrick, G. M. *SHELXTL VS.1, Software Reference Manual*; Bruker AXS, Inc.: Madison, WI, 1997. (b) Sheldrick, W. S.; Morr, M. *Acta Crystallogr., Sect. B* **1981**, *37*, 733−734.
(14) Zhang, L.; Xu, S.; Zhou, Y.; Zheng, X.; Yu, C.; Shi, Z.; Hassan, S. *CrystEngComm* **2011**, *13*, 6511−6519.
(15) (a) Gałdecka, E.; Gałdecki, Z.; Gawryszewska, P.; Legendziewicz, J. *New J. Chem.* **2000**, *24*, 387−391. (b) Biju, S.; Reddy, M. L. P.; Alan, H. C.; Kalyan, V. V. *Cryst. Growth Des.* **2009**, *9*, 3562−3569. (c) Tong, F.; Sun, Z.-G.; Chen, K.; Zhu, Y.-Y.; Wang, W.-N.; Jiao, C.-Q.; Wang, C.-L.; Li, C. *Dalton Trans.* **2011**, *40*, 5059−5065.
(16) Balaban, A. T. *From Chemical Topology to Three-Dimensional Geometry*; Plenum Press: New York, 1997.
(17) Spek, A. L. *PLATON. A Multi-purpose Crystallographic Tool*; Utrecht University: Utrecht, The Netherlands, 2001.
(18) Huang, Q.; Wu, X.; Lu, J. *Polyhedron* **1997**, *16*, 833−838.
(19) Santana, H.-d.; Toni, L. R. M.; Luis, O. d. B.; Zaia, C. T. B. V.; Rosa, M.; Zaia, D. A. M. *Geoderma* **2006**, *136*, 738−750.
(20) Cabeza, A.; Ouyang, X.; Sharma, C. V. K.; Aranda, M. A. G.; Bruque, S.; Clearfield, A. *Inorg. Chem.* **2002**, *41*, 2325−2333.
(21) Lucky, M. V.; Sivakumar, S.; Reddy, M. L. P.; Paul, A. K.; Natarajan, S. *Cryst. Growth Des.* **2011**, *11*, 857−864.
(22) Paula, C. R.; Santos, S.; Luís, C.-S.; Filipe, A. A. P.; Ferreira, R. A. S.; Rocha, J.; Carlos, L. D.; Helena, I.; Nogueira, S. *Inorg. Chem.* **2010**, *49*, 3428−3440.
(23) Xu, B.; Yan, B. *Spectrochim. Acta, Part A* **2007**, *66*, 236−242.
(24) Tang, X.-L.; Dou, W.; Chen, S.-W.; Dang, F.-F.; Liu, W.-S. *Spectrochim. Acta, Part A* **2007**, *68*, 349−353.
(25) Soares-Santos, P. C. R.; Cunha-Silva, L.; Paz, F. A. A.; Ferreira, R. A. S.; Rocha, J.; Carlos, L. D.; Nogueira, H. I. S. *Inorg. Chem.* **2010**, *49*, 3428−3440.
(26) (a) Dexter, D. L. *J. Chem. Phys.* **1953**, *21*, 836−841. (b) Sato, S.; Wada, M. *Bull. Chem. Soc. Jpn.* **1970**, *43*, 1955−1962. (c) Li, X.; Wang, C. Y.; Hu, H. M. *Inorg. Chem. Commun.* **2008**, *11*, 345−348. (d) Li, C.; Quan, Z.; Yang, J.; Yang, P. P.; Lin, J. *Inorg. Chem.* **2007**, *46*, 6329−6337.
(27) Zhang, H. J.; Yan, B.; Wang, S. B.; Ni, J. Z. *J. Photochem. Photobiol. A* **1997**, *109*, 223−228.
(28) Wang, Y. B.; Zheng, X. J.; Zhuang, W. J.; Jin, L. P. *Eur. J. Inorg. Chem.* **2003**, 1355−1360.
(29) (a) Burrow, C. E.; Burchell, T. J.; Lin, P. H.; Habib, F.; Wernsdorfer, W.; Clerac, R.; Murugesu, M. *Inorg. Chem.* **2009**, *48*, 8051−8053. (b) Chen, W. T.; Fukuzumi, S. *Inorg. Chem.* **2009**, *48*, 3800−3807. (c) Viswanathan, S.; Bettencourt-Dias, A. D. *Inorg. Chem.* **2006**, *45*, 10138−10146. (d) Liu, X. G.; Zhou, K.; Dong, J.; Zhu, C. J.; Bao, S. S.; Zheng, L. M. *Inorg. Chem.* **2009**, *48*, 1901−1905.
(30) (a) Li, Z. Y.; Dai, J. W.; Wang, N.; Qiu, H. H.; Yue, S. T.; Liu, Y. L. *Cryst. Growth Des.* **2010**, *10*, 2746−2751. (b) Wang, C. G.; Xing, Y. H.; Li, Z. P.; Li, J.; Zeng, X. Q.; Ge, M. F.; Niu, S. Y. *Cryst. Growth Des.* **2009**, *9*, 1525−1530. (c) Liu, M. S.; Yu, Q. Y.; Cai, Y. P.; Su, C. Y.; Lin, X. M.; Zhou, X. X.; Cai, J. W. *Cryst. Growth Des.* **2008**, *8*, 4083−4091.
(31) (a) Steemers, F. J.; Verboom, W.; Reinhoudt, D. N.; Tol, E. B. V.; Verhoeven, J. W. *J. Am. Chem. Soc.* **1995**, *117*, 9408−9414. (b) Latva, M.; Takalob, H.; Mukkala, V. M.; Matachescuc, C.; Rodriguez-Ubisd, J. C.; Kankarea, J. *J. Lumin.* **1997**, *75*, 149−169. (c) Cui, Y. J.; Yue, Y. F.; Qian, G. D.; Chen, B. L. *Chem. Rev.* **2012**, *2*, 1126−1162. (d) Lucky, M. V.; Sivakumar, S.; Reddy, M. L. P.; Paul, A. K.; Natarajan, S. *Cryst. Growth Des.* **2011**, *11*, 857−864. (e) Bünzli, J. C. G. *Chem. Rev.* **2010**, *110*, 2729−2755. (f) Archer, R. D.; Chen, H. *Inorg. Chem.* **1998**, *37*, 2089.
(32) (a) Wong, K. L.; Law, G. L.; Yang, Y. Y.; Wong, W. T. *Adv. Mater.* **2006**, *18*, 1051. (b) Kłonkowski, A. M.; Lis, S.; Pietraszkiewicz, M.; Hnatejko, Z.; Czarnobaj, K.; Elbanowski, M. *Chem. Mater.* **2003**, *15*, 656−663.
(33) (a) de Lill, D. T.; de Bettencourt-Dias, A.; Cahill, C. L. *Inorg. Chem.* **2007**, *46*, 3960−3965. (b) Soares-Santos, P. C. R.; Cunha-Silva, L.; Paz, F. A. A.; Ferreira, R. A. S.; Rocha, J.; Trindade, T.; Carlos, L. D.; Nogueira, H. I. S. *Cryst. Growth Des.* **2008**, *8*, 2505−2516.
(34) (a) Xiao, M.; Selvin, P. R. *J. Am. Chem. Soc.* **2001**, *123*, 7067−7073. (b) Comby, S.; Imbert, D.; Chauvin, A.; Bunzli, J. G.; Charbonniere, L. J.; Ziessel, R. F. *Inorg. Chem.* **2004**, *43*, 7369−7379.
(35) Werts, M. H. V.; Jukes, R. T. F.; Verhoeven, J. W. *Phys. Chem. Chem. Phys.* **2002**, *4*, 1542−1548.